

Deep Learning for landmarking on morphometry anatomical images

Le Van Linh^{a,c,*}, Beurton-Aimar Marie^{a,1}, Zemmari Akka^a, Parisey Nicolas^{b,1}

^a*University of Bordeaux, 351, cours de la Libération, 33405 Talence, France*

^b*UMR 1349 IGEPP, BP 35327, 35653 Le Rheu, France*

^c*Dalat University, Dalat, Lamdong, Vietnam*

Abstract

In recent years, deep learning, which has been introduced in the middle of the previous century for artificial intelligence, has risen strongly because of improvements in the computation both in memory size and computing time with GPU programming. Deep learning, specially Convolutional Neural Network (CNN), has been applied to solve the problems in different domains such as computer vision, speech recognition, or languages translation, . . . In computer vision, CNN has been used to classify the images into different categories, or to detect the object in images/videos, or to predict the key points of the objects in the images, . . . and it has brought the amazing achievements. In this work, we propose a CNN model to predict the key points (landmarks) on 2D anatomical biological images, specify beetle's images. Our proposed network is trained and evaluated on a dataset includes the images of collecting from 293 beetles. During the experiments, the network is tested in two ways: training from scratch and applying fine-tuning. The quality of predicted landmarks is evaluated by comparing with the manual landmarks which provided by the biologists. The obtained results are considered to be statistically good enough to replace the manual landmarks for the different morphometry analysis.

Keywords: Landmarks, deep learning, fine-tuning, CNN

*Corresponding author

Email address: van-linh.le@labri.fr (Le Van Linh)

¹both authors contributed equally to this work.

1. Introduction

Key points detection has a wide use and becomes a critical in image analysis of different domains, such as: In geosciences, the key points can be used to recognize the seabed by extracting and comparing the landmarks from sonar images at different times; or computer vision, they are fundamental to detect the human face or human pose; in biology, the topography of the objects of an organism can be measured if we have enough the number of landmarks. Landmarks, or *key points*, or *points of interest*, are the points on the image that store important information about the shape of the object, *for example*, the left and right corners of eyes are two important points to detect the human eyes. Depending on the object, the number of landmarks may be different, as well as their position can be defined along the outline of the object or inside the object, i.e. the landmarks on *Drosophila* wings [1] are stayed on the veins of the wings, but the landmarks on human ears [2] can be located on the ear edge or inside the pinnae of the ears.

Early methods [3, 4, 5] mainly focused on the low level-vision of the image by applying the image processing techniques, and segmentation is most often the first and the most important step. This task remains a bottleneck to compute the features of an image. In some cases, the interested object is easy to extract and can be analyzed by applying the well-known image analysis procedures. Nevertheless, we can not apply the same procedure for un-segmentable images. It really becomes a challenge on the complex images. Luckily, the appearance of deep learning has seen huge success in handwritten digit recognition, speech, images classification and detecting objects in images. Now, an interesting thing is how to use deep learning for landmark detecting, which can be considered as the local characteristic of the image. Our motivation to design a CNN model that able to extract the landmarks on images (even it is segmentable or un-segmentable), which will be used to replace for the previous procedures.

The main idea consists of the designing and training a CNN [6] on a dataset with manual landmarks. Like other CNNs, the features are extracted by us-

ing a group of different layer types (i.e. convolutional layer, pooling layer,...) followed by some dense layers to provide the prediction of the network. After designing, the proposed model will be trained on the dataset includes the images which are taken from 293 beetles. For each beetle, the biologists have taken images of five parts: *left and right mandibles, head, elytra, and pronotum* (Figs.1a, 2a, 3a, 4a, 5a). All the images are presented in the RGB color model with two dimensions. Along with each image, a set of landmarks has been marked by experts which can be used as ground truth to evaluate the predicted landmarks (Figs.1b, 2b, 3b, 4b, 5b). During the experiments, the proposed network has been trained on the dataset by applying two strategies. In the first strategy, the network is trained from scratch on each dataset; while in the second strategy, the training process has been modified to include a fine-tuning [7] stage. Besides, the value of Root Mean Square Error (RMSE) is used to compute the losses during two experiment processes. For more information about the model, you can see at our repository on GitHub: https://github.com/linhlelandlu/CNN_Beetles_Landmarks.

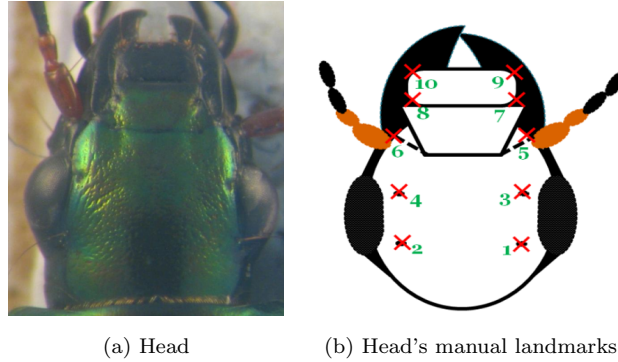


Figure 1: The **head** anatomical of beetle and its manual landmarks

The rest of this paper is organized as followed: Section 2 discusses the related works about determining the landmarks on 2D images. Then, a short overview about CNN and its components will be introduced in Section 3. Section 4 gives another approaches to augment the dataset. Section 5 shows the procedure

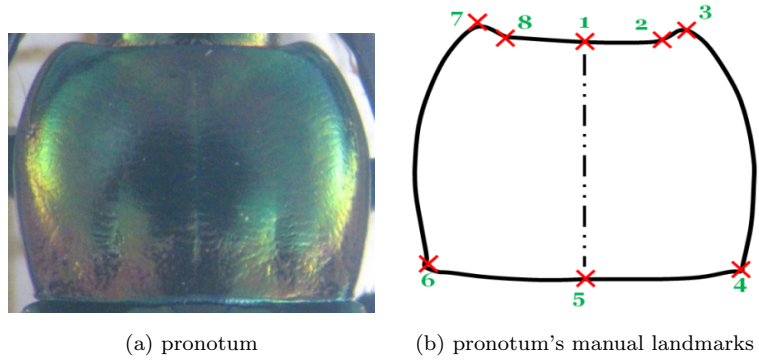


Figure 2: The **pronotum** anatomical of beetle and its manual landmarks

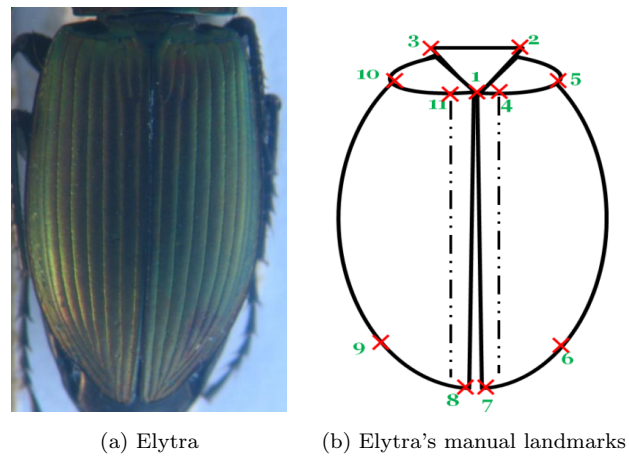


Figure 3: The **elytra** anatomical of beetle and its manual landmarks

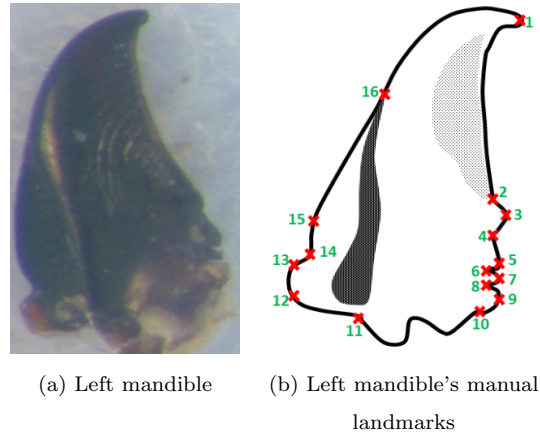


Figure 4: The **left mandible** anatomical of beetle and its manual landmarks

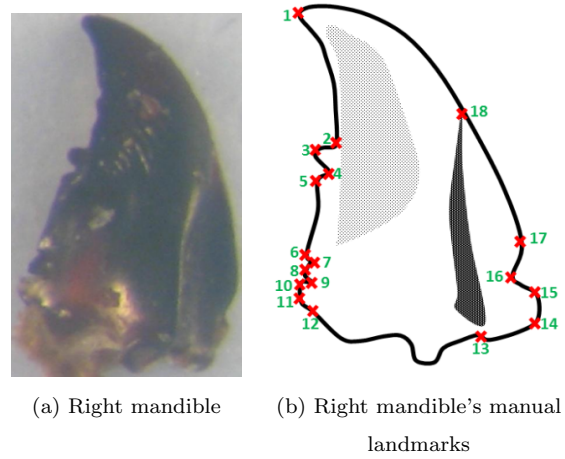


Figure 5: The **right mandible** anatomical of beetle and its manual landmarks

of designing the network model. The first experiment of the network on each dataset is presented in Section 6. Section 7 presents a modification of training process and its experiment on datasets. Finally, the conclusion is given in Section 8.

55 2. Related works

Deep learning [8] has been introduced in the middle of the previous century for artificial intelligence application but it has encountered several problems to take real-world cases such as memory or computing time. Luckily, the improvements of computing capacities, both in memory size and in computing
60 time with GPU programming, have opened new perspective for deep learning. In recent years, deep learning architectures are known as the solutions for the tasks in computer vision. Especially in image analysis, CNNs, which consist of convolutional layers, pooling layers, full connected layers, are used to solve the classification or recognition tasks. For example, LeNet [9] has been known as
65 the first architecture of CNN to read the zip codes and digits. It had a standard structure stacked convolutional layers (normalization and max-pooling) are followed by one or more full-connected layers. From this architecture, many models have been proposed to improve the accuracy as well as computing times in recent years. That must be mentioned to AlexNet [10], ZFNet [11], GoogLeNet
70 [12], VGGNet [13], or ResNet [14]. Besides, deep learning has been obtained the achievement in other domains such as **image recognition** [12, 15, 16], **speech recognition** [17, 18], **language translation** [19, 20], **natural language processing** [8, 21, 22],

Besides object classification or recognition, **key points detection** is another
75 task in image analysis. Early methods of machine learning have been achieved good results. These methods are basically divided into two groups: the regression-based methods and template fitting methods. A regression-based method predicts landmark locations by regression using image features [23, 24, 25]. While a template fitting method builds a template to fit with

the input image, then the landmarks are setting [26, 27, 28]. With the come-
back of deep learning, CNN has been used to predict the landmarks on 2D
and it has gained better results. Yi Sun et al. [29] have proposed a cascaded
CNNs to predict the facial points on the human face. Their model includes
the networks which have separated into three levels of the cascade. The net-
works recognize the human face from the global to the local view to increasing
the accuracy of predicted key points. Zhanpeng Zhang et al. [30] proposed
a *Tasks-Constrained Deep Convolutional Network* to optimize facial landmarks
detection. Their model detected the facial landmarks with a set of related tasks
such as head pose estimation, gender classification, age estimation, or facial
attribute inference. Shaoli Huang et al. [31] introduced a coarse-fine network,
which composed of several coarse detector branches, to locate the keypoints
and to estimate the human pose. Cintas et al. [2] has introduced a network to
predict the landmarks on human ears (Fig. 6). After training, the network has
the ability to detect 45 landmarks on human ears.

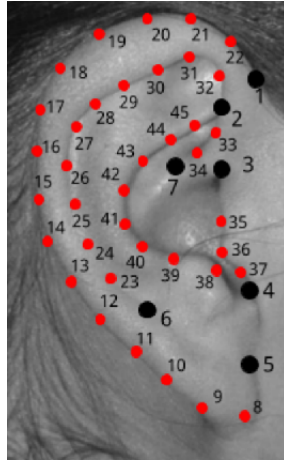


Figure 6: Landmarks on human ear in study of Cintas et al. [2]

As an association with the biologist, we study to develop an automatic
method for predicting the landmarks on beetle's anatomical (Figs.1a, 2a, 3a,
4a, 5a). In the past, locating landmarks on biological images is mainly using

image processing techniques where the object in the image is easily to segment. For example, in a previous work [32], we have applied a series of algorithms to
100 detect the landmarks automatically on beetles mandibles which are considered as the easied objects to segment (with an quality enough good for our need). In that work, the landmarks have been detected by registering two segmentations of images and then, using SIFT descriptor to refine the location of predicted landmarks. After the experiment, we have obtained good enough results on
105 mandibles. Unfortunately, we have observed that the method did not provide good results when the segmentation is not precise, i.e. on pronotum or elytra images. This is explained why we have turned the automatically landmarking into another stage without any segmentation step. Using CNN for landmarking seems that a good choice for un-segmentable images.

110 3. Overview of Convolutional Neural Network

CNN is a feedforward network which takes the information following one direction from the inputs to the outputs. Currently, CNNs have many different variations, i.e. AlexNet [10], GoogLeNet [33], ResNet [14], but in general, it consists of convolutional and pooling layers which are stacked together to con-
115 volve and to down-sample the input. Then, they are followed by one or more fully connected layers to give the decision as the output of the network.

Fig. 7 shows an example of a CNN for classification problem. The network inputs directly an image to several stages of convolutional and pooling layers. Then, the representation is feed into three fully connected layers. A dropout
120 layer is inserted after the second fully connected layer (it is repsented by some blue nodes). Finally, the last fully connected layer gives the category label for the input image. This architecture could be seen as a popular one that we can find from the literature [9, 10]. However, several architectures have been proposed recurrently to improve the accuracy or to decrease the computation
125 costs. In this section, we will mention to the most popular layers in a CNN: convolutional layers, pooling layers, and fully connected layers.

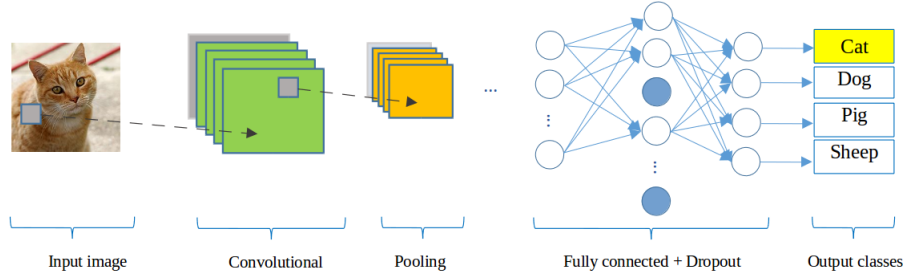


Figure 7: A CNN network for classification problem

Convolutional (CONV) layers: use as a feature extractor by applying some learnable weights on the input images. The input image is convolved with the learnable weights in order to compute the new feature maps; then, the convolved results are sent through a nonlinear activation. In convolutional layer, the neurons are arranged into feature maps. All the neurons within a feature map have constrained to be equal; however, different features maps within the same convolutional layer have different weights so that several features can be extracted at each location of an input image.

Pooling (POOL) layers : are mostly used to down-sampling the size of the input with the purpose to reduce the spatial resolution of the feature map to reduce the computation cost. Initially, it was common practice to use average pooling which propagates the average of all the input to the next layer. However, in more recent models [10, 34, 16], max pooling which propagates the maximum value (selecting the largest value) with a receptive field to the next layer. Fig. 8 illustrates the differences between max and average pooling. Give an input image of size 4×4 , if applying a 2×2 filter and stride of two is applied, the output will be had the size of 2×2 for both cases. However, the value in each element of the output is different because the max pooling outputs the maximum values of the filter region, while average pooling outputs the average value of the same region.

Dropout [35] is a specific layer, it is used to prevent the over-fit of a neural network. The term dropout mentions dropping the out units and their

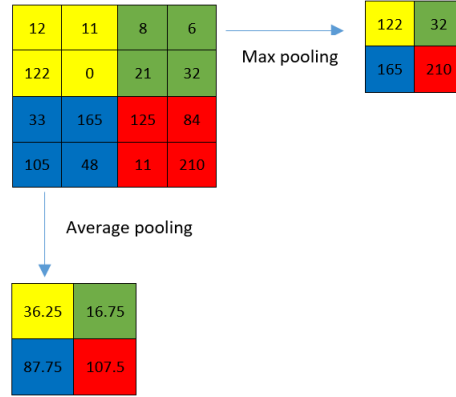


Figure 8: The results of different pooling

connections (incoming and outgoing) of a layer in the network. The units are
 150 dropped randomly with a probability p independent with other units. The idea
 of dropout is not limited to feed-forward neural nets. Applying dropout tech-
 nique will make the network become a collection of thinned networks because a
 number of units are dropped randomly at each presentation of training phase.
 So, training a neural network with dropout looks like training a collection of
 155 the thinned networks. Normally, the dropouts layers are placed after the fully
 connected layers, but it is possible to use dropout after the pooling layers with
 creating some kind of images noise augmentation.

Fully connected (FC) layers: are usually followed the convolutional and pool-
 ing layers which used to extract the abstract feature representations. A CNN
 160 may have one or more fully connected layers. It interprets the feature represen-
 tations and performs a function of high-level reasoning (i.e. giving classification
 score) by applying the activation functions. In practice, the last fully connected
 layer refers to the output of the network and choosing the activation function is
 depended on which kind of problem that network solve, i.e. we usually softmax
 165 activation function for a classification problem but it is not useful in a support
 vector machine.

To solve a problem by using deep learning, besides designing the network

architecture then training dataset is also a very important thing. The nature of deep learning algorithm is training the model on dataset repeatedly to reach the best accuracy. So, providing a large dataset will provide more learning cases for the model and it will clearly improve the learnable of the network. Unfortunately, data in practice has usually not enough. So, some methods have been applied to generate the fake data with the purpose to augment the dataset (i.e. rotate, translate, flip the images). Our case is also not an exception, we work on a small dataset of beetles with 293 images for each part. This number is really modest to apply deep learning. In the next section, we describe the procedure to augment the dataset before coming to design the architectures.

4. Data augmentation

A characteristic of machine learning and deep learning is using a volume dataset to train the model. Of course, we do not always have enough data for training in practice. One way to solve this problem is to create fake data from real data and to add it to the training set. Dataset augmentation has been a particularly effective technique for a specific problem. For example, in images classification problem, the operations like translating, rotating or scaling the images have also effective. The fake images may be generated by translating (rotating or scaling) in each direction. Besides, injecting noise in the input can also see as a form of data augmentation.

Our dataset includes 293 images of beetles (for each anatomical part). All the images are taken with the same camera in the same condition with a resolution of (3264×2448) . Each image has a set of manual landmarks provided by biologists, i.e, each pronotum has 8 landmarks, each head has 10 landmarks. Applying CNNs to train each part with a small number of images to reach good results is impossible. So, we need to augment the dataset before training the networks. Firstly, we have found that the original solution of the images (3264×2448) are heavy for the neural network. For performance considerations, in most of CNNs [2, 6, 29], the size of the input is limited to (256×256) pixels,

so we have decided to down-sampling the images to a new resolution (256×192) (to respect the ratio between x and y). Of course, the coordinates of manual landmarks have been also scaled to fit with the new resolution of the images.

200 In the usual way, the transformations have been used to augment the dataset (i.e rotation, translation,...) but the analysis of image by CNN is most often translation and rotation invariant. Therefore, two other procedures have been imaged to increase the number of images in the dataset (256×192).

The first procedure is to change the value of a color channel in the original image to generate a new image. According to that, a constant is added to one of the RGB channels each time it is used for training. Each constant is sampled in a uniform distribution $\in [1, N]$ to obtain a new value caped at 255. For example, Fig. 9 shows an example when we added a constant $c = 10$ to each channel of an original image. Following this way, we can generate three version

210 from an image.

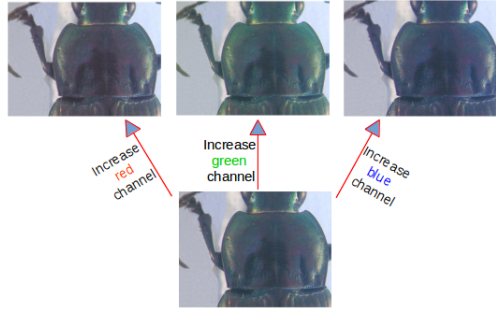


Figure 9: A constant $c = 10$ has been added to each channel of an original image

In the second procedure, we have applied the opposite procedure to the first one. Instead of adding the value, we separate the channels of RGN into three gray-scale images as the network works on single channel images (Fig. 10). At the end of the processes, we are able generate six versions from an original

215 image. In total, we have $293 \times 7 = 2051$ images for each anatomical part of beetle (an original image and six generated images). However, we have not used all images for training and validation. So, we have chosen 260 original images

and their generations (1820 images) of each dataset for training and validation processes, the remaining images (33 original images) are used for test process.

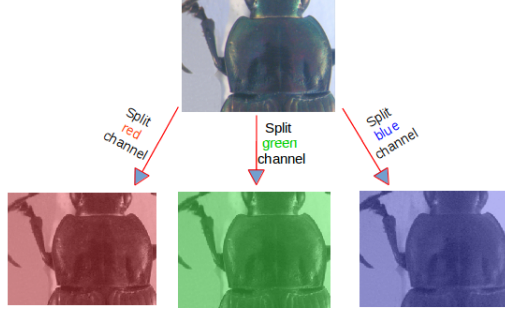


Figure 10: Three channels (red, green, blue) are separated from original image

220 In practical, to obtain a fast convergence during the computing, it is useful to normalize the brightness of the images to $[0, 1]$ instead of $[0, 255]$ and the coordinates of the landmarks have been also normalized [36].

5. Network architectures designing

From the beginning of CNN, LeNet [9] can be considered as the first one, which has used to classify digits on hand-written numbers on cheques. The network is very simple by stack together the convolutional layers and max-pooling layers followed by full connected layers. Because of the limit of the resources at that time, this model is also constrained by the availability of computing. Until 2012, when computing resources are improved, AlexNet [10] was born and it has won the challenge by reducing the top-5 error in ImageNet challenge. AlexNet had a similar architecture as LeNet but it was deeper, bigger. Besides, the activation functions have been changed from Sigmoid [37] to ReLU [38] which have been proved more improvement in computing time. Additional, it had supplement the dropout layers to control overfitting. Based on the idea of the improvement, we have tried to design an architecture for landmarking on beetle images. This work is beginning with trying three network models before deciding the final architecture. Like other CNN models, we have employed the

classical layers to construct the models, i.e., convolutional layers, maximum pooling layers, dropout layers and full-connected layers.

240 The first architecture is very classical one, it receives an image with the size of $(1 \times 192 \times 256)$ as the input. Then, the network consists on three repeated strcutre of a convolutional layers followed by a maximum pooling layers. Most CNNs, the hyperparameters of convolutional layers have been set to increase the depth of the images from the first layer to the last layer. That is reflected in
245 the setting of the number of filters at each convolutional layer. So, the depths of convolutional layers increase from 32, 64, and 128 with different size of the kernels: (3×3) , (2×2) and (2×2) , respectively. Inserting pooling layers after a convolutional layers is a common periodcally. The pooling layer effects to progressively reduce the spatial size of the representation to reduce the number
250 of parameters, computation in the network, and it also controls over-fitting. The operations of pooling layers independent on every depth slice of the input. The most common form is a pooling layer with filters of size (2×2) and a stride of 2. It downsamples every depth by 2 along width and height of the input. Therefore, all the kernels of maximum pooling layers have the same size of (2×2)
255 with a stride of 2 as usual. At the end of the model, three full-connected layers have been added to extract the global relationship between the features and to procedure the outputs. The first of two full-connected layers are set to non-linearity to make sure these nodes interact well and take into account all possible dependencies at the feature level. The outputs of the full-connected layers
260 are 500, 500 and 16. The output of the last full-connected layer corresponds to the coordinates $(x$ and $y)$ of 8 landmarks which we would like to predict. Fig. 11 shows details of the first model: The orange rectangles represent for convolutional layers while the yellow rectangles represent for maximum pooling layers and three full-connected layers with their parameters are presented at the
265 end of the model.

The second architecture is modified from the first model. The layers are kept the same as the first one but the outputs of the first of two full-connected layers are changed from 500 (in the first model) to 1000 (Fig. 12). Increasing the value

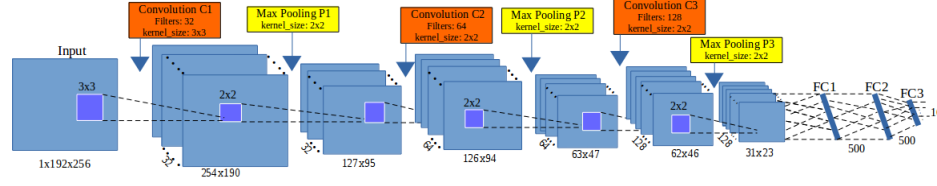


Figure 11: The architecture of the first model

at full-connected layers is hoping to obtain more features from convolutional
 270 layer and to prevent the over-fitting.

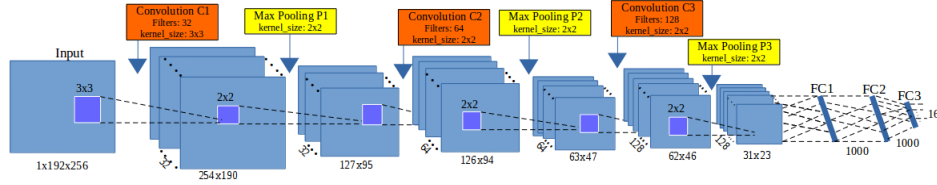


Figure 12: The architecture of the second model

To build the third architecture, we have used the definition of *elementary block*. An elementary block is defined as a sequence of convolution (C_i), maximum pooling (P_i) and dropout (D_i) layers (Fig. 13). This significantly reduces overfitting and gives major improvements over other regularization methods
 275 [35]. The idea of dropout is to include some variations between different runs. During training phase, dropout samples are done from an exponential number of different “thinned” network. At test phase, it is easy to approximate the effect of averaging the prediction of all thinned networks by simply using a single unthinned network with smaller weights. So, we have modified the architecture
 280 by combining some *elementary blocks*.

Fig. 14 illustrates the layers in the third architecture. For our purpose, we have assembled **3 elementary blocks**. The parameters for each layer in each elementary block are as below, the list of values follows the order of elementary blocks ($i = [1..3]$):

- 285 • CONV layers:

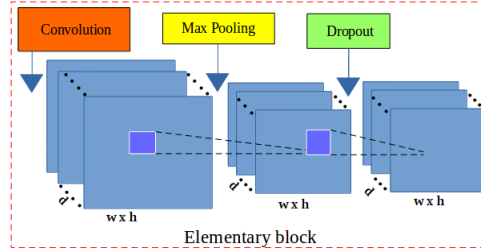


Figure 13: The layers in an elementary block

- Number of filters: 32, 64, and 128
- Kernel filter sizes: (3×3) , (2×2) , and (2×2)
- Stride values: 1, 1, and 1
- No padding is used for CONV layers

290

- POOL layers:

- Kernel filter sizes: (2×2) , (2×2) , and (2×2)
- Stride values: 2, 2, and 2
- No padding is used for POOL layers

- DROP layers:

295

- Probabilities: 0.1, 0.2, and 0.3

Three full-connected layers (FC) are kept the same as the second architecture: FC1 and FC2 have 1000 outputs, the last full-connected layer (FC3) has 16 outputs. As usual, a dropout layer is inserted between FC1 and FC2 with a probability equal to 0.5.

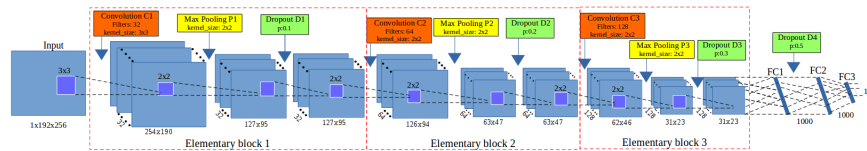


Figure 14: The architecture of the third model

300 The core of CNN is training over iteration. There are many ways to optimize
the learning algorithm, but gradient descent [36] is currently a good choice to
establish the way of optimizing the loss in neural network. The core idea is
following the gradient until we statify with the results will remain the same. So,
we have chosen gradient descent in the backward phase to update the values
305 of learnable parameters and to increase the accuracy of the network. The net-
works are designed with a small sharing learning rate and a momentum. The
learning rate is initialized at 0.03 and stopped at 0.00001, while the momentum
is updated from 0.9 to 0.9999. Their values are updated over training time to
fit with the number of epochs ². The implementation of the architectures have
310 been done on Lasagne framework [39] by Python.

6. Experiments and results

Before widely applying to all anatomical parts, we have firstly tried with
pronotum part to evaluate the performance. The networks have been trained
in 5,000 epochs on Ubuntu machine by using NVIDIA TITAN X cards. The
315 set of images that used for training and validation are merged together. During
the training, the images are chosen randomly from the dataset with a ratio of
60% for training and 40% for validation. The training step takes into account
a pair of information (*images, manual landmarks coordinates*) as training data.
In the context of deep learning, landmark prediction can be seen as a regres-
320 sion problem. So, we have used Root Mean Square Error (RMSE) to compute
the loss of implemented architectures. At the test phase, images without land-
marks are given to the trained network to produce output coordinates of the
predicted landmarks. The results then evaluated by comparing with the manual
landmarks coordinates provided by biologists which have been seen as ground
325 truth.

Fig. 15 shows the training errors and the validation errors during traning

²An epoch is a single pass through the full training set

phase of the first architecture. The blue curve presents the RMSE errors of training process while green curve is the validation errors. Clearly, over-fitting has appeared in the first model. The training losses are able to decrease but the validation losses are stable. In the second model (Section 5), we have modified the parameters of full-connected layers to prevent the over-fitting but it seems that this solution is still not suitable.

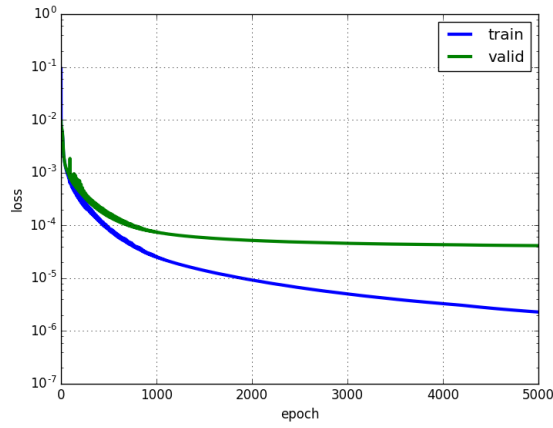


Figure 15: The training and validation losses of the first model

Then, we have continued to train the third model on the same dataset of pronotum images. Fig. 16 illustrates the losses during the training of the third model. As the same meaning in Fig. 15, the blue line is training loss, the green line is validation loss. In the opposite with two previous models, the losses are different (far) from the beginning but after several epochs, the loss values become more proximate and the over-fitting problem has been solved. This proves that adding dropout layers to build the elementary blocks have been effects to prevent over-fitting and contributory improve the accuracy of the model. *So, we have decided to keep the architecture of the third model for our landmarking problem.*

In order to have the predicted landmarks for all pronotum images (instead of only 33 images), we have applied *cross-validation* to choose the test images,

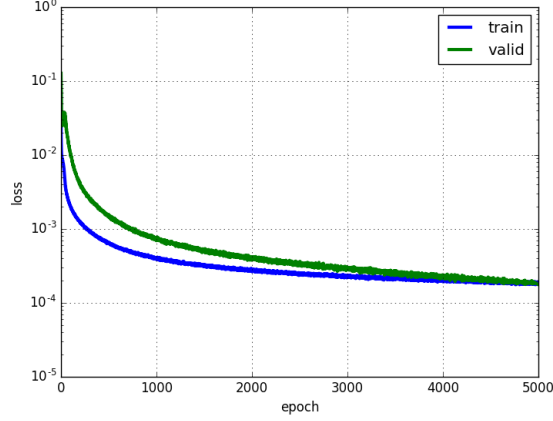


Figure 16: The training and validation losses of the third model

345 called *round*. For each time, we have chosen a different fold of 33 images as testing images, the remaining images are used as training and validation images (293/33 \approx 9 rounds). Following that, the network will be trained with different datasets, then the trained model will be used to predicted the lanmarks on the images in the corresponding test set. Table. 1 resumes the losses of 9 rounds
 350 when we trained the third model on pronotum images. Clearly, the training loss/validation loss among rounds are not so large and the RMSE values are looking pretty good ($\approx 1.7 - 2.1$ pixels).

To evaluate the coordinates of predicted landmarks, the correlation metrics have been computed the correlation between the manual landmarks and their
 355 corresponding predicted one. Table. 2 shows the correlation scores of 3 metrics (using *scikit-learn* [40]), i.e, coefficient of determination (r^2), explained variance (EV), and Pearson correlation. All of three metrics have the same possibility. The best score is 1.0 if the correlation data is good, lower values are worse. It means that our predicted coordinates are very close with the ground truth.
 360 However, the measure is not enough good to provide a useful result to biologists. Moreover standing on the side of image processing, we are looking forward to seeing the predicted coordinates than the statistical results.

Round	Training loss	Validation loss
1	0.00018	0.00019
2	0.00019	0.00021
3	0.00019	0.00026
4	0.00021	0.00029
5	0.00021	0.00029
6	0.00019	0.00018
7	0.00018	0.00018
8	0.00018	0.00021
9	0.00020	0.00027

Table 1: The losses during training the third model on pronotum images

Metric	$\mathbf{r^2}$	EV	Pearson
Score	0.9952	0.9951	0.9974

Table 2: Correlation scores between manual landmarks and predicted landmarks

The main goal of computing is to predict the coordinates of landmarks, so the distances (in pixels) between the coordinates of manual landmarks and corresponding predicted landmarks have been taken into account on all images. Then, the average of distances are computed by landmarks. Table. 3 shows the average distances by landmarks on all images of pronotum dataset. With images of resolution 256×192 , we can consider that an error of 1% corresponds to 2 pixels that could be an acceptable error. Unhappily, our results exhibit average distance of 4 pixels in the best case, landmark 1 and more than 5 pixels, landmark 6. Other error distances are more than 2% pixels.

Fig. 17 shows the distribution of the distances on the first landmark of all images. The accuracy based on the distance in each image can be separated into three spaces: the images have the distance less than average value (4 pixels): 56.66%; the images have the distance from average value to 10 pixels (5% acceptable errors): 40.27%; and the images have the distance greater than 10

Landmark	Distance (in pixels)
1	4.002
2	4.4831
3	4.2959
4	4.3865
5	4.2925
6	5.3631
7	4.636
8	4.9363

Table 3: The average distances on all images per landmark on pronotum images.

pixels: 3.07%.

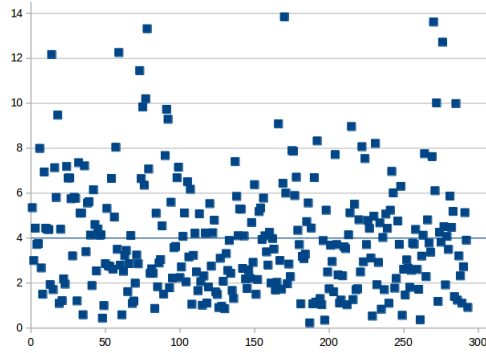


Figure 17: The distribution of the distances on the first landmark. The blue line is the average value of all distances.

To illustrate this purpose, Fig. 18 shows the predicted landmarks on two test images. One can note that even some predicted landmarks (Fig. 18a) are closed
390 to the manual ones, in some case (Fig. 18b) the predicted ones are far from the expect results. This result explains why the average distance by landmarks are enough good while some predicted landmarks are so far from the manual one. So, the next step has been dedicated to the improvement of these results.

From the success of the third architecture on pronotum dataset, we apply the

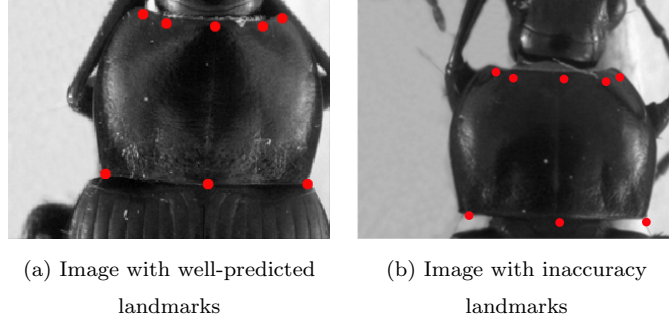


Figure 18: The predicted landmarks, in red, on the images in test set.

385 same procedures (data augmentation, training, . . .) on other parts of beetle: *left*
and right mandibles, elytra and head. However, we have modified the number of
output of the last full-connected layer to adapt with each dataset before training.
According, the values at the last full-connected layer are set to 32, 36, 22 and
20 outputs corresponds to 16, 18, 11 and 10 landmarks on left mandible, right
390 mandible, elytra and head, respectively. Of course, we have also applied cross-
validation to select testing data to get all predicted landmarks for all images
in each dataset. Then, the quality of predicted landmarks are evaluated by
comparing with the corresponding manual landmarks (distance computation).
Table. 4 shows the average distances on each landmark of elytra, head, left and
395 right mandibles anatomical, respectively. Comparing with the average distances
on the pronotum part, the average distances on elytra and head parts are very
close, but a little bit far on the mandible parts.

7. Resulting improvement by fine-tuning

The proposed network (third architecture) presented in Section 5 have been
400 trained from scratch on five datasets of beetles (left mandible, right mandible,
pronotum, elytra, and head). At the first step, the network was able to predict
the landmarks on the images. But as we have discussed, even if the strength
of the correlation seems to validate the results, when we display the predicted

Landmark	Distance (in pixels)			
	Right mandible	Left mandible	Elytra	Head
1	9.4981	9.1267	3.8669	5.528
2	7.1657	6.7198	3.973	5.1609
3	7.242	6.8704	3.9166	5.3827
4	7.0436	6.7719	3.8673	5.0345
5	7.1599	7.125	4.0151	4.8393
6	7.5699	6.9441	4.8426	4.4516
7	7.4251	7.3158	5.2125	4.7937
8	7.6636	7.4142	5.4685	4.5322
9	7.7906	7.5846	5.2692	5.1412
10	8.0197	7.6349	4.0709	5.0564
11	8.314	7.6873	3.9896	-
12	8.1564	8.4248	-	-
13	8.8879	7.9983	-	-
14	9.1842	7.4919	-	-
15	8.7875	7.7903	-	-
16	8.3141	8.5198	-	-
17	8.2866	-	-	-
18	8.8928	-	-	-

Table 4: The average distances on all images per landmark on left mandible, right mandible, elytra and head images.

landmarks on the images, the quality of the predicted coordinates are also not
405 enough precise, and the average error are also still high (of course, we have the
distances are higher than the average distances).

In order to reach more acceptable results for biologists, we have broadened
model with another step of deep learning: **transfer learning**. That is a method
enables to re-uses the model developed for a specific task/dataset to lead another
410 task (called *target task*) with another dataset. This process allows rapid process
and improves the performance of the model on the target task [41]. The most
popular example has been given with the project ImageNet of Google [42] which
has labeled several millions of images. The obtained parameter values which can
be used in another context to classify another dataset, eventually very different
415 dataset [43]. The name of this procedure to re-use parameters to pretrain a
model is currently called **fine-tuning**.

Fine-tuning does not only replace and retrain the model on the new dataset
but also fine-tunes the weights of a trained model by continuing the backprop-
agation. Unfortunately, some rapid tests have shown that re-using ImageNet
420 features has not been relevant for our application. We have designed a way to
reproduce the method with our own data. It is worth noting that of course the
size of data to pre-train has drastically decreased. For our pre-training step, the
network has been trained on the whole dataset including the images of three
parts of beetle *i.e pronotum, elytra and head*. Then, the trained model has been
425 used to fine-tune and test on each dataset.

7.1. Data preparation and training

The images training dataset is combined from the images of three sets:
pronotum, elytra, and head (after augmentation). When applying the train-
ing from the scratch, we have used cross-validation to select the data (9 folds).
430 It means that for each dataset, we have some different training data and corre-
sponding testing data. So, the images that use to train the model are just select
from one of the folds in each dataset. Specifically, we have taken 1,820 images
of each part. In total, it includes 5,460 images ($260 \times 7 \times 3$).

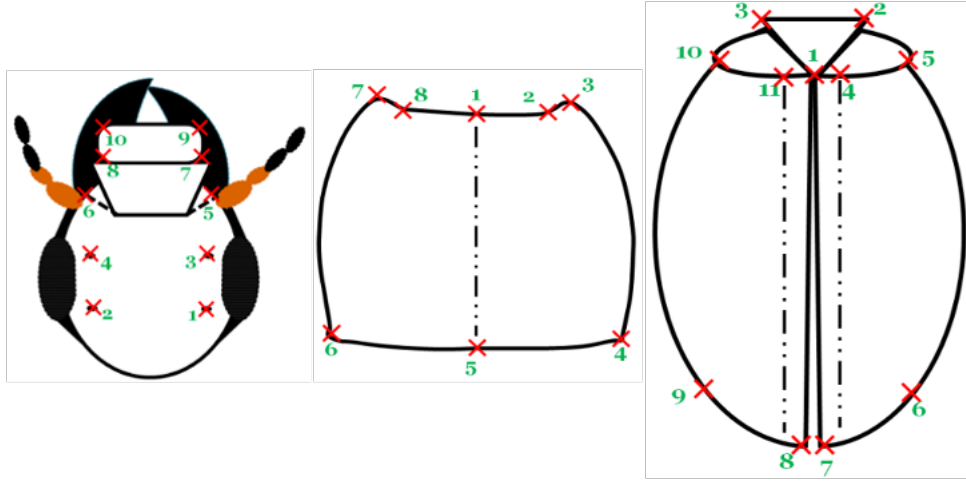


Figure 19: A presentation of head, pronotum and elytra part with corresponding manual landmarks

However, another problem has been appeared when we combined the images
 435 from different dataset. That is the different number of landmarks on each part:
 8 landmarks on pronotum part, 10 landmarks on head part, and 11 landmarks on
 elytra part. Fig. 19 shows the position of the landmarks on each part. Because
 of the meaning of landmarks on each anatomical part for biologists, we cannot
 insert the landmarks arbitrary. So, we have decided to keep the landmarks
 440 on pronotum as reference and to remove the landmarks on elytra and head
 parts instead of adding. We kept 8 (landmarks) as a reference number, then we
 have removed the supernumerary when it is unnecessary. Specifically, we have
 removed three landmarks on the elytra part (1^{st} , 6^{th} , 9^{th}), and two landmarks
 on the head part (5^{th} , 6^{th}).

445 During training the proposed architecture on the combined dataset, the pa-
 rameters of the network (learning rate, momentum, ...) are kept the same as
 training from scratch but the number of epochs are increased to 10,000 instead
 of 5,000 to achieve better learning on the parameters (weights). Additional,
 we have shuffled the training set. Because the neural network learns the faster
 450 from the most unexpected sample. It is advisable to choose a sample at each

iteration that is the most unfamiliar to the system. Shuffling the examples will be helped the model works with different anatomical parts rather than the same anatomical samples in each training time.

7.2. Fine-tuning on each dataset

455 The combined dataset then used to train the third architecture with 16 outputs (8 landmarks). Then, the trained model is used to fine-tuning on each dataset. To compare the result with the previous one, we have also fine-tuned the trained model with different dataset by applying cross-validation. Firstly, we consider on the losses during fine-tuning. *For example*, Table. 5, 7, 9 show
 460 the losses during fine-tuning on pronotum, elytra, and head dataset, respectively. Comparing with the losses when we trained the model from scratch, *i.e.* on pronotum, the validation losses of all round in this scenario have been significantly decreased (around 40%).

On each part, the landmarks are predicted on the test images. Then, the average error based on the distances between predicted and corresponding manual
 465 landmarks have been also computed. Tables. 6, 8, 10, 11, and 12 show the average distances per landmark on pronotum, elytra, head, left and right mandibles dataset, respectively. **From scratch** columns remind the previously average distances. **Fine-tune** columns present the new average distances after applying
 470 fine-tuning on each part. It is clearly shown that the result of predicted landmarks with the help of fine-tuning is more precise than training from scratch. For example, the average distance at each landmark has decreased. Additional, when comparing the average distances between two processes, the worse case of fine-tuning process is still better than the best case of training from scratch.

475 In another view, Fig. 20 shows the comparison of the average distance distributions on each dataset in two procedures (from scratch and fine-tuning). In which:

- **Blue** curves: present for the average distances on each landmarks when we train the model from scratch.

Round	Training loss	Validation loss
1	0.00019	0.00009
2	0.00018	0.00010
3	0.00018	0.00010
4	0.00019	0.00008
5	0.00019	0.00009
6	0.00018	0.00008
7	0.00019	0.00008
8	0.00018	0.00006
9	0.00018	0.00009

Table 5: The losses during fine-tuning model on pronotum dataset

Round	Training loss	Validation loss
1	0.00020	0.00006
2	0.00020	0.00006
3	0.00021	0.00006
4	0.00021	0.00006
5	0.00019	0.00006
6	0.00019	0.00006
7	0.00018	0.00005
8	0.00020	0.00006
9	0.00019	0.00006

Table 7: The losses during fine-tuning model on elytra dataset

#LM	From scratch	Fine-tune
1	4.00	2.49
2	4.48	2.72
3	4.30	2.65
4	4.39	2.77
5	4.29	2.49
6	5.36	3.05
7	4.64	2.68
8	4.94	2.87

Table 6: The average error distance per landmark of two processes on pronotum images

#LM	From scratch	Fine-tune
1	3.87	2.34
2	3.97	2.27
3	3.92	2.27
4	3.87	2.25
5	4.02	2.27
6	4.84	3.14
7	5.21	3.14
8	5.47	3.29
9	5.27	3.42
10	4.07	2.49
11	3.99	2.30

Table 8: The average error distance per landmark of two processes on elytra images

Round	Training loss	Validation loss
1	0.00022	0.00007
2	0.00022	0.00007
3	0.00023	0.00008
4	0.00023	0.00008
5	0.00022	0.00008
6	0.00023	0.00007
7	0.00022	0.00008
8	0.00023	0.00007
9	0.00024	0.00008

Table 9: The losses during fine-tuning model on head dataset

#LM	From scratch	Fine-tune
1	5.53	3.03
2	5.16	2.94
3	5.38	2.96
4	5.03	2.88
5	4.84	2.76
6	4.45	2.67
7	4.79	2.29
8	4.53	2.20
9	5.14	2.57
10	5.06	2.44

Table 10: The average error distance per landmark of two processes on head images

- **Orange** curves: describe for the average distance on each landmark when we fine-tune the trained model.
- **Black** curves (in the case of left and right mandibles): illustrate for the average distances when we applied the image processing procedures to predict the landmarks on segmentable images.

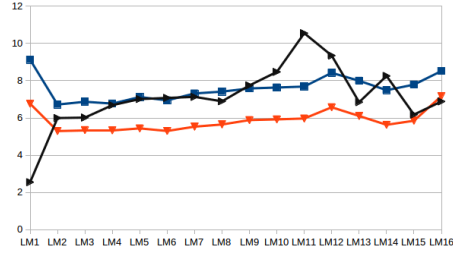
The fine-tuning process has improved the results of the proposed architecture on both 5 datasets: left, right mandible, pronotum, elytra and head. All the average distances are significantly decreased. Specially, the results have been improved $\approx 26.9\%$ on left mandible, $\approx 22.8\%$ on right mandible, $\approx 40.3\%$ on pronotum, $\approx 39.8\%$ on elytra, and $\approx 46.4\%$ on head part based on considering the average distances per landmark. Addition, in the cases of pronotum and head part, even if we plus the average distance and its standard deviation, the results are also less than the result when we trained the model from scratch. For segmentable images, we have a comparison between the results of deep learning and early method where we have applied image processing techniques to predict

#LM	From scratch	Fine-tune
1	9.1267	6.7655
2	6.7198	5.2952
3	6.8704	5.3468
4	6.7719	5.332
5	7.125	5.4391
6	6.9441	5.3004
7	7.3158	5.5314
8	7.4142	5.6486
9	7.5846	5.8864
10	7.6349	5.9245
11	7.6873	5.972
12	8.4248	6.5755
13	7.9983	6.1067
14	7.4919	5.6307
15	7.7903	5.8522
16	8.5198	7.174

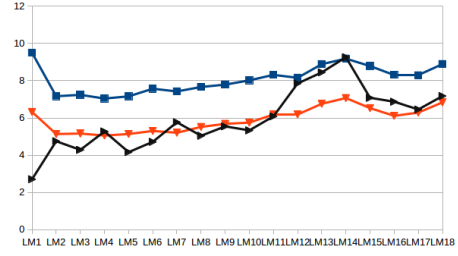
Table 11: The average error distance per landmark of two processes on left mandible images

#LM	From scratch	Fine-tune
1	9.4981	6.3236
2	7.1657	5.1347
3	7.242	5.1613
4	7.0436	5.0537
5	7.1599	5.1372
6	7.5699	5.301
7	7.4251	5.2064
8	7.6636	5.5168
9	7.7906	5.6858
10	8.0197	5.7495
11	8.314	6.1975
12	8.1564	6.1898
13	8.8879	6.7612
14	9.1842	7.0694
15	8.7875	6.5293
16	8.3141	6.1147
17	8.2866	6.2881
18	8.8928	6.8367

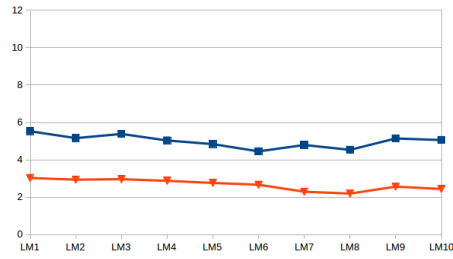
Table 12: The average error distance per landmark of two processes on head images



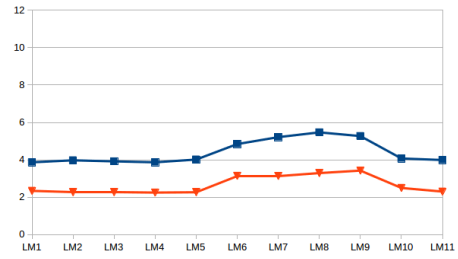
(a) Left mandible



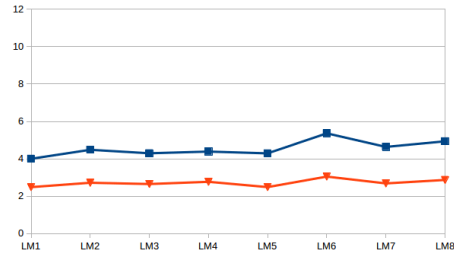
(b) Right mandible



(c) Head



(d) Elytra



(e) pronotum

Figure 20: The distribution of average distances on each landmark of each beetle's anatomical

the landmarks. Clearly, the result with fine-tuning has improved the location of estimated landmarks. Even the average distances which obtained from scratch training are still high but they are more stable than the results from the early method: most of the average distance(or landmarks) of left mandibles are less than the results of the early method, while the average distances are very closed in the case of right mandibles.

To compare the results between image processing procedures and deep learning, we have run the test on an image of all parts in both methods. Then, we have calculated the distances between manual and predicted landmarks (in both cases). Fig. 21 shows the locations of manual and predicted landmarks on each beetle's part from both two methods. In these images, the **red points** present the manual landmarks, the **yellow points** are estimated landmarks from image processing procedures and the **green points** are predicted landmarks which provided by deep learning. Fig. 22 shows the distances of each part that we have obtained. In these charts, the **blue lines** present the distances when we apply the calculation on image processing procedures; the **orange and yellow lines** show the distances with deep learning: training from scratch and fine tuning, respectively.

As described in [32], we have combined some image processing procedures to output the predicted landmarks and this has become also a disadvantage of this method. If one procedure of them provides a bad result, it will affect the final result, i.e. if the result of segmentation step is bad, it seems that can not provide the output. In all beetle's anatomical, the mandibles are considered as the easy case to segment because the images are clear (they just contains the mandibles); while other parts are much noise, besides the main objects they have also the subcomponents of beetle, i.e. leg, antennae, That explains why we have obtained good results on mandibles but bad results on head, elytra, and pronotum part when applying the image processing procedures. In the opposite side, the results with deep learning, either training from scratch or fine-tuning, are very stable (Fig. 22). In the case of mandibles which have good results from image processing techniques then the results from deep learning are not much

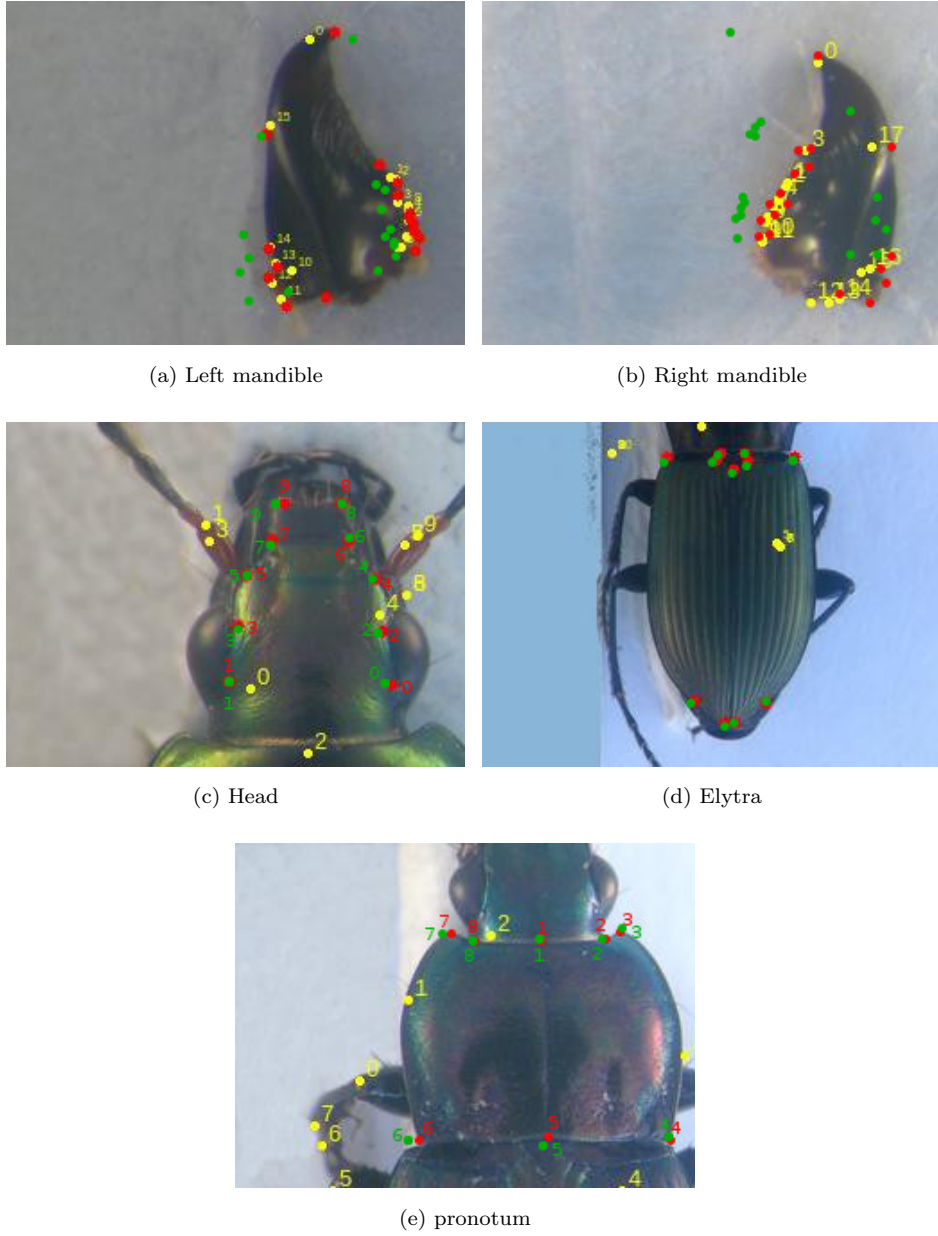


Figure 21: The presentation of manual and predicted landmarks on each beetle's part by applying two methods: image processing procedures and deep learning

difference.

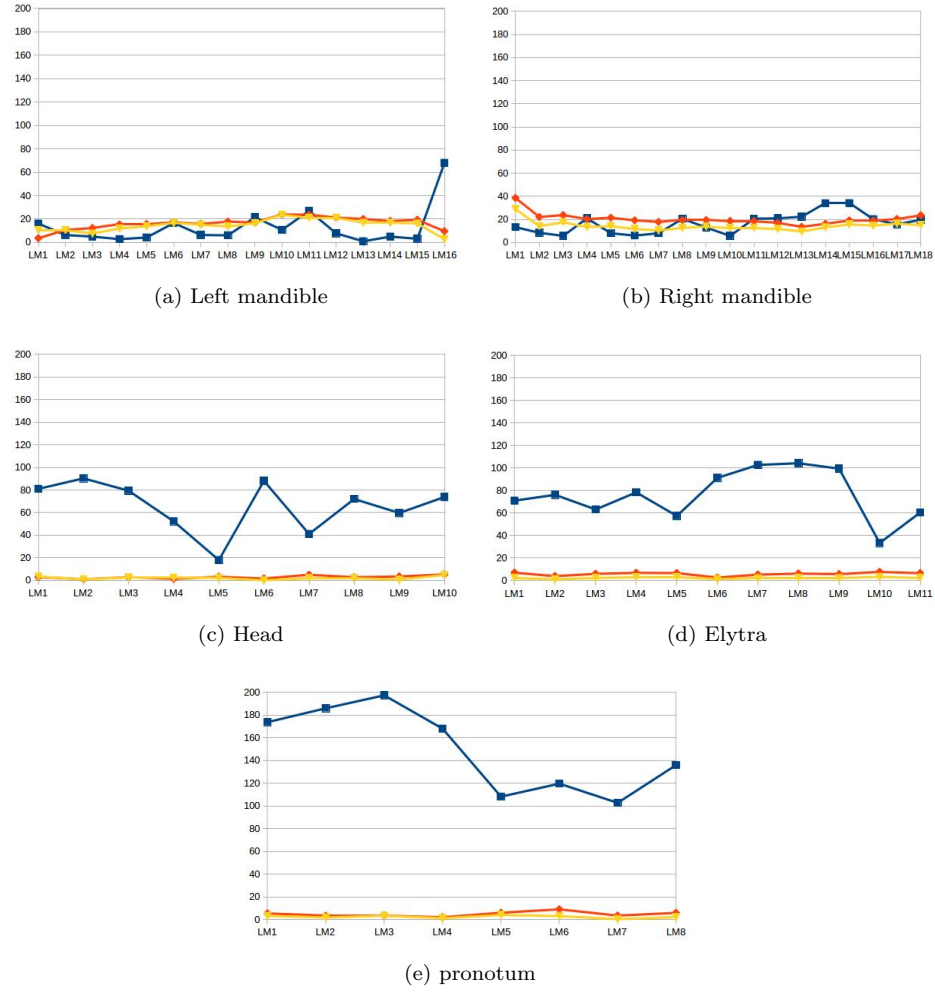


Figure 22: The distances between manual and predicted landmarks of a test image when applying different techniques of each beetle's anatomical

8. Conclusion

In this work, we have presented how to apply convolutional neural network to predict the landmark on 2D anatomical images of beetles. After going through many trial models, we have presented a convolutional neural network for automatic detection landmarks on anatomical images of beetles which includes the repeated of some elementary blocks (an elementary block consists of a convolutional layer, a max pooling layer, and a dropout layer) followed by fully connected layers. Then, the proposed model have been trained and tested by using two strategies: *train from scratch* and *fine-tuning*.

In our case, the size of dataset is limited. Therefore, we have applied the image processing techniques to augment dataset. The predicted landmarks have been evaluated by calculating the distance between manual landmarks and corresponding predicted landmarks. Then, the average of distance errors on each landmarks has been considered.

The results have been shown that using the convolutional network to predict the landmarks on biological images leads to satisfying results without need for segmentation step on the object of interest. The best set of estimated landmarks has been obtained after a step of fine-tuning using the whole set of images that we have for the project, i.e. about all beetle parts. The quality of prediction allows using automatic landmarking to replace the manual ones.

References

- [1] A. Sonnenschein, D. VanderZee, W. R. Pitchers, S. Chari, I. Dworkin, Supporting material and data for "an image database of drosophila melanogaster wings for phenomic and biometric analysis" (2015). doi: 10.5524/100141.
- [2] C. Cintas, et al., Automatic ear detection and feature extraction using geometric morphometrics and convolutional neural networks, IET Biometrics 6 (3) (2016) 211–223.

- 555 [3] D. G. Lowe, Distinctive image features from scale-invariant keypoints, *International journal of computer vision* 60 (2) (2004) 91–110.
- [4] H. Bay, T. Tuytelaars, L. Van Gool, Surf: Speeded up robust features, in: *European conference on computer vision*, Springer, 2006, pp. 404–417.
- [5] S. Palaniswamy, N. A. Thacker, C. P. Klingenberg, Automatic identification
560 of landmarks in digital images, *IET Computer Vision* 4 (4) (2010) 247–260.
- [6] Y. LeCun, K. Kavukcuoglu, C. Farabet, Convolutional networks and applications in vision, in: *Circuits and Systems (ISCAS)*, *Proceedings of 2010 IEEE International Symposium on*, IEEE, 2010, pp. 253–256.
- [7] J. Yosinski, J. Clune, Y. Bengio, H. Lipson, How transferable are features
565 in deep neural networks?, in: *Advances in neural information processing systems*, 2014, pp. 3320–3328.
- [8] Y. LeCun, Y. Bengio, G. Hinton, Deep learning, *Nature* 521 (7553) (2015) 436–444.
- [9] Y. LeCun, L. Bottou, Y. Bengio, P. Haffner, Gradient-based learning applied to document recognition, *Proceedings of the IEEE* 86 (11) (1998)
570 2278–2324.
- [10] A. Krizhevsky, I. Sutskever, G. E. Hinton, Imagenet classification with deep convolutional neural networks, in: *Advances in neural information processing systems*, 2012, pp. 1097–1105.
- [11] M. D. Zeiler, R. Fergus, Visualizing and understanding convolutional networks, in: *European conference on computer vision*, Springer, 2014, pp. 818–833.
575
- [12] C. Szegedy, et al., Going deeper with convolutions, *Cvpr*, 2015.
- [13] K. Simonyan, A. Zisserman, Very deep convolutional networks for large-scale image recognition, *arXiv preprint arXiv:1409.1556*.
580

- [14] K. He, X. Zhang, S. Ren, J. Sun, Deep residual learning for image recognition, in: Proceedings of the IEEE conference on computer vision and pattern recognition, 2016, pp. 770–778.
- [15] C. Farabet, C. Couprie, L. Najman, Y. LeCun, Learning hierarchical features for scene labeling, IEEE transactions on pattern analysis and machine intelligence 35 (8) (2013) 1915–1929.
- [16] H. Li, Z. Lin, X. Shen, J. Brandt, G. Hua, A convolutional neural network cascade for face detection, in: Proceedings of the IEEE Conference on Computer Vision and Pattern Recognition, 2015, pp. 5325–5334.
- [17] T. Mikolov, et al., Strategies for training large scale neural network language models, in: Automatic Speech Recognition and Understanding (ASRU), 2011 IEEE Workshop on, IEEE, 2011, pp. 196–201.
- [18] G. Hinton, et al., Deep neural networks for acoustic modeling in speech recognition: The shared views of four research groups, IEEE Signal Processing Magazine 29 (6) (2012) 82–97.
- [19] S. Jean, K. Cho, R. Memisevic, Y. Bengio, On using very large target vocabulary for neural machine translation, arXiv preprint arXiv:1412.2007.
- [20] I. Sutskever, O. Vinyals, Q. V. Le, Sequence to sequence learning with neural networks, in: Advances in neural information processing systems, 2014, pp. 3104–3112.
- [21] R. Collobert, J. Weston, L. Bottou, M. Karlen, K. Kavukcuoglu, P. Kuksa, Natural language processing (almost) from scratch, Journal of Machine Learning Research 12 (Aug) (2011) 2493–2537.
- [22] R. Collobert, J. Weston, A unified architecture for natural language processing: Deep neural networks with multitask learning, in: Proceedings of the 25th international conference on Machine learning, ACM, 2008, pp. 160–167.

- [23] M. Valstar, B. Martinez, X. Binefa, M. Pantic, Facial point detection using boosted regression and graph models, in: Computer Vision and Pattern Recognition (CVPR), 2010 IEEE Conference on, IEEE, 2010, pp. 2729–2736.
- [24] M. Dantone, J. Gall, G. Fanelli, L. Van Gool, Real-time facial feature detection using conditional regression forests, in: Computer vision and pattern recognition (CVPR), 2012 IEEE conference on, IEEE, 2012, pp. 2578–2585.
- [25] X. P. Burgos-Artizzu, P. Perona, P. Dollár, Robust face landmark estimation under occlusion, in: Proceedings of the IEEE International Conference on Computer Vision, 2013, pp. 1513–1520.
- [26] T. F. Cootes, G. J. Edwards, C. J. Taylor, Active appearance models, IEEE Transactions on Pattern Analysis & Machine Intelligence (6) (2001) 681–685.
- [27] X. Liu, Generic face alignment using boosted appearance model, in: Computer Vision and Pattern Recognition, 2007. CVPR'07. IEEE Conference on, IEEE, 2007, pp. 1–8.
- [28] X. Yu, J. Huang, S. Zhang, W. Yan, D. N. Metaxas, Pose-free facial landmark fitting via optimized part mixtures and cascaded deformable shape model, in: Proceedings of the IEEE International Conference on Computer Vision, 2013, pp. 1944–1951.
- [29] Y. Sun, X. Wang, X. Tang, Deep convolutional network cascade for facial point detection, in: Proceedings of the IEEE conference on computer vision and pattern recognition, 2013, pp. 3476–3483.
- [30] Z. Zhang, et al., Facial landmark detection by deep multi-task learning, in: European Conference on Computer Vision, Springer, 2014, pp. 94–108.

- [31] S. Huang, M. Gong, D. Tao, A coarse-fine network for keypoint localization,
 635 in: The IEEE International Conference on Computer Vision (ICCV), Vol. 2,
 2017.
- [32] V. L. Le, M. Beurton-Aimar, A. Krahenbuhl, N. Parisey, MAELab: a
 framework to automatize landmark estimation, in: WSCG 2017, Plzen,
 Czech Republic, 2017.
 640 URL <https://hal.archives-ouvertes.fr/hal-01571440>
- [33] C. Szegedy, W. Liu, Y. Jia, P. Sermanet, S. Reed, D. Anguelov, D. Er-
 han, V. Vanhoucke, A. Rabinovich, Going deeper with convolutions, corr
 abs/1409.4842, URL <http://arxiv.org/abs/1409.4842>.
- [34] D. Ciregan, U. Meier, J. Schmidhuber, Multi-column deep neural networks
 645 for image classification, in: Computer Vision and Pattern Recognition
 (CVPR), 2012 IEEE Conference on, IEEE, 2012, pp. 3642–3649.
- [35] N. Srivastava, G. E. Hinton, A. Krizhevsky, I. Sutskever, R. Salakhutdinov,
 Dropout: a simple way to prevent neural networks from overfitting., Journal
 of machine learning research 15 (1) (2014) 1929–1958.
- 650 [36] Y. A. LeCun, et al., Efficient backprop, in: Neural networks: Tricks of the
 trade, Springer, 2012, pp. 9–48.
- [37] J. Han, C. Moraga, The influence of the sigmoid function parameters on the
 speed of backpropagation learning, in: International Workshop on Artificial
 Neural Networks, Springer, 1995, pp. 195–201.
- 655 [38] V. Nair, G. E. Hinton, Rectified linear units improve restricted boltzmann
 machines, in: Proceedings of the 27th international conference on machine
 learning (ICML-10), 2010, pp. 807–814.
- [39] S. Dieleman, et al., Lasagne: First release. (Aug. 2015). doi:10.5281/
 zenodo.27878.
 660 URL <http://dx.doi.org/10.5281/zenodo.27878>

- [40] P. et al, Scikit-learn: Machine learning in python, Journal of machine learning research 12 (Oct) (2011) 2825–2830.
- [41] L. Torrey, J. Shavlik, Transfer learning, Handbook of Research on Machine Learning Applications and Trends: Algorithms, Methods, and Techniques 1 (2009) 242.
- [42] J. Deng, et al., ImageNet: A Large-Scale Hierarchical Image Database, in: CVPR09, 2009.
- [43] J. Margeta, et al., Fine-tuned convolutional neural nets for cardiac mri acquisition plane recognition, Computer Methods in Biomechanics and Biomedical Engineering: Imaging & Visualization 5 (5) (2017) 339–349. arXiv:<https://doi.org/10.1080/21681163.2015.1061448>, doi: 10.1080/21681163.2015.1061448.
URL <https://doi.org/10.1080/21681163.2015.1061448>